LETTERS

High molecular gas fractions in normal massive star-forming galaxies in the young Universe

L. J. Tacconi[1], R. Genzel[1,2], R. Neri[3], P. Cox[3], M. C. Cooper[4], K. Shapiro[5], A. Bolatto[6], N. Bouché[1], F. Bournaud[7], A. Burkert[8], F. Combes[9], J. Comerford[5], M. Davis[5], N. M. Förster Schreiber[1], S. Garcia-Burillo[10], J. Gracia-Carpio[1], D. Lutz[1], T. Naab[8], A. Omont[11], A. Shapley[12], A. Sternberg[13] & B. Weiner[4]

Stars form from cold molecular interstellar gas. As this is relatively rare in the local Universe, galaxies like the Milky Way form only a few new stars per year. Typical massive galaxies in the distant Universe formed stars an order of magnitude more rapidly[1,2]. Unless star formation was significantly more efficient, this difference suggests that young galaxies were much more molecular-gas rich. Molecular gas observations in the distant Universe have so far largely been restricted to very luminous, rare objects, including mergers and quasars[3–5], and accordingly we do not yet have a clear idea about the gas content of more normal (albeit massive) galaxies. Here we report the results of a survey of molecular gas in samples of typical massive-star-forming galaxies at mean redshifts $<z>$ of about 1.2 and 2.3, when the Universe was respectively 40% and 24% of its current age. Our measurements reveal that distant star forming galaxies were indeed gas rich, and that the star formation efficiency is not strongly dependent on cosmic epoch. The average fraction of cold gas relative to total galaxy baryonic mass at $z = 2.3$ and $z = 1.2$ is respectively about 44% and 34%, three to ten times higher than in today's massive spiral galaxies[6]. The slow decrease between $z \approx 2$ and $z \approx 1$ probably requires a mechanism of semi-continuous replenishment of fresh gas to the young galaxies.

Direct observations of molecular gas in galaxies as a function of cosmic epoch are required to understand how galaxies have turned their gas into stars. To explore the evolution of cold gas fractions, we selected two samples of star-forming galaxies (SFGs) spanning similar ranges in stellar mass and star formation rates: one at redshift $z \approx 1.2$ ($t_o \approx 5.5$ Gyr, where t_o is the time since the Big Bang) and the other at $z \approx 2.3$ ($t_0 \approx 3$ Gyr). With recent improvements in instrumental sensitivity, we can now sample the massive tail of the typical, or 'normal', SFGs in this epoch (Supplementary Information section 1). These 'main-sequence' galaxies are believed to have high (40–70%) duty cycles of star formation, and most are probably not 'starbursts' in a brief period of activity, such as major dissipative mergers[1,2]. Figure 1 displays the source-integrated spectra in the CO $J = 3$–2 transition for 19 of the galaxies observed, 10 at $z \approx 2$ and 9 at $z \approx 1$. For 14 SFGs we have solid ($>4\sigma$ r.m.s.) detections in both redshift ranges, and for the first time for $z > 2$ SFGs. In five galaxies the emission is marginally or not detected, or may be continuum rather than line emission. Table 1 summarizes the observed and derived galaxy properties.

For EGS 1305123 ($z = 1.12$) and EGS 1207881 ($z = 1.17$), we also obtained high quality spatially resolved maps with FWHM (full-width at half-maximum) resolutions of 0.65″ and 1″, respectively. Figure 2c shows the integrated CO 3–2 emission in EGS 1305123, superposed on an optical image from the Hubble Space Telescope (HST). This map resolves for the first time the cold molecular gas distribution in a clearly non-merging high-z SFG. This system looks like a scaled-up version (in terms of star formation rate and gas mass) of normal $z \approx 0$ gas-rich disk galaxies. In the optical images, EGS 1305123 is a nearly face-on, large spiral disk. The clumpy CO emission extends over the entire disk, with a strong concentration of gas near the nucleus and innermost spiral arms (Fig. 2c). CO velocity channel maps (Fig. 2a, b) exhibit giant clumps with inferred gas masses of $\sim 5 \times 10^9\, M_\odot$ (where $M_\odot$ indicates solar mass), intrinsic diameters $<$2–4 kpc, gas surface densities $\geq 500\, M_\odot\, \mathrm{pc}^{-2}$ and velocity dispersions $\sigma \approx 20\, \mathrm{km\, s}^{-1}$. These clumps are correlated with, but typically separated by >1 kpc from, the brightest nearby optical H II regions (similar to $z \approx 0$ spirals[7,8]). They probably represent loose conglomerates of several giant molecular clouds that are not yet resolved by our measurements, rather than a single, gravitationally stabilized, giant cloud, since the velocity dispersions are too low for their masses. These clumps are similar to but larger than conglomerates of molecular gas in $z \approx 0$ spiral galaxies, which have masses of $\sim(1\text{–}3) \times 10^7\, M_\odot$, diameters of 500 pc, surface densities of $\sim 100\, M_\odot\, \mathrm{pc}^{-2}$ and velocity dispersions of $\sim$6–12 $\mathrm{km\, s}^{-1}$ (ref. 7). The CO dynamics trace an ordered rotating disk pattern with maximum intrinsic rotation velocity $v_{\mathrm{d,max}} \approx 200\, \mathrm{km\, s}^{-1}$ (Fig. 2d–f). The inferred ratio of rotational velocity to line-of-sight velocity dispersion, σ, in the outer disk is $v_{\mathrm{d,max}}/\sigma \approx 10$, implying a molecular gas disk that is fairly thin but somewhat more turbulent than in local spirals[7,8]. The CO dynamics in EGS 1207881 are also consistent with that of a large rotating disk.

The lower resolution observation galaxies, EGS 13004291, EGS 13017614, EGS 13003805 and EGS 12011767, all exhibit double-peaked line profiles with a spatial offset between the red and blue emission peaks, as expected for rotation in an extended disk (Supplementary Fig. 2). This interpretation is consistent with the HST images (Supplementary Fig. 2; images are available at http://tkserver.keck.hawaii.edu/egs/egsSurvey/egs_acsDownloads.php).

For Q2324-BX 610 at $z = 2.21$ we detect a velocity gradient (Supplementary Fig. 2), which is consistent with the well defined rotation pattern in Hα line emission tracing ionized gas[9]. No published high resolution imaging or spectroscopy is available for the other $z \approx 2$ galaxies in our sample. On the basis of Hα kinematics of 62 $z \approx 2$

[1]Max-Planck-Institut für extraterrestrische Physik (MPE), Giessenbachstr. 1, 85748 Garching, Germany. [2]Department of Physics, Le Conte Hall, University of California, Berkeley, California 94720, USA. [3]IRAM, 300 Rue de la Piscine, 38406 St Martin d'Heres, Grenoble, France. [4]Steward Observatory, 933 N. Cherry Ave., University of Arizona, Tucson, Arizona 85721-0065, USA. [5]Department of Astronomy, Campbell Hall, University of California, Berkeley, California 94720, USA. [6]Department of Astronomy, University of Maryland, College Park, Maryland 20742-2421, USA. [7]Service d'Astrophysique, DAPNIA, CEA/Saclay, F-91191 Gif-sur-Yvette Cedex, France. [8]Universitätssternwarte der Ludwig-Maximiliansuniversität, Scheinerstr. 1, D-81679 München, Germany. [9]LERMA, Observatoire de Paris, 61 Av. de l'Observatoire, F-75 014 Paris, France. [10]Observatorio Astronómico Nacional-OAN, Apartado 1143, 28800 Alcalá de Henares-Madrid, Spain. [11]Institut d'Astrophysique de Paris, CNRS and Université Pierre and Marie Curie, 98 bis boulevard Arago, 75014 Paris, France. [12]Department of Physics and Astronomy, University of California, Los Angeles, California 90095-1547, USA. [13]School of Physics and Astronomy, Tel Aviv University, Tel Aviv 69978, Israel.

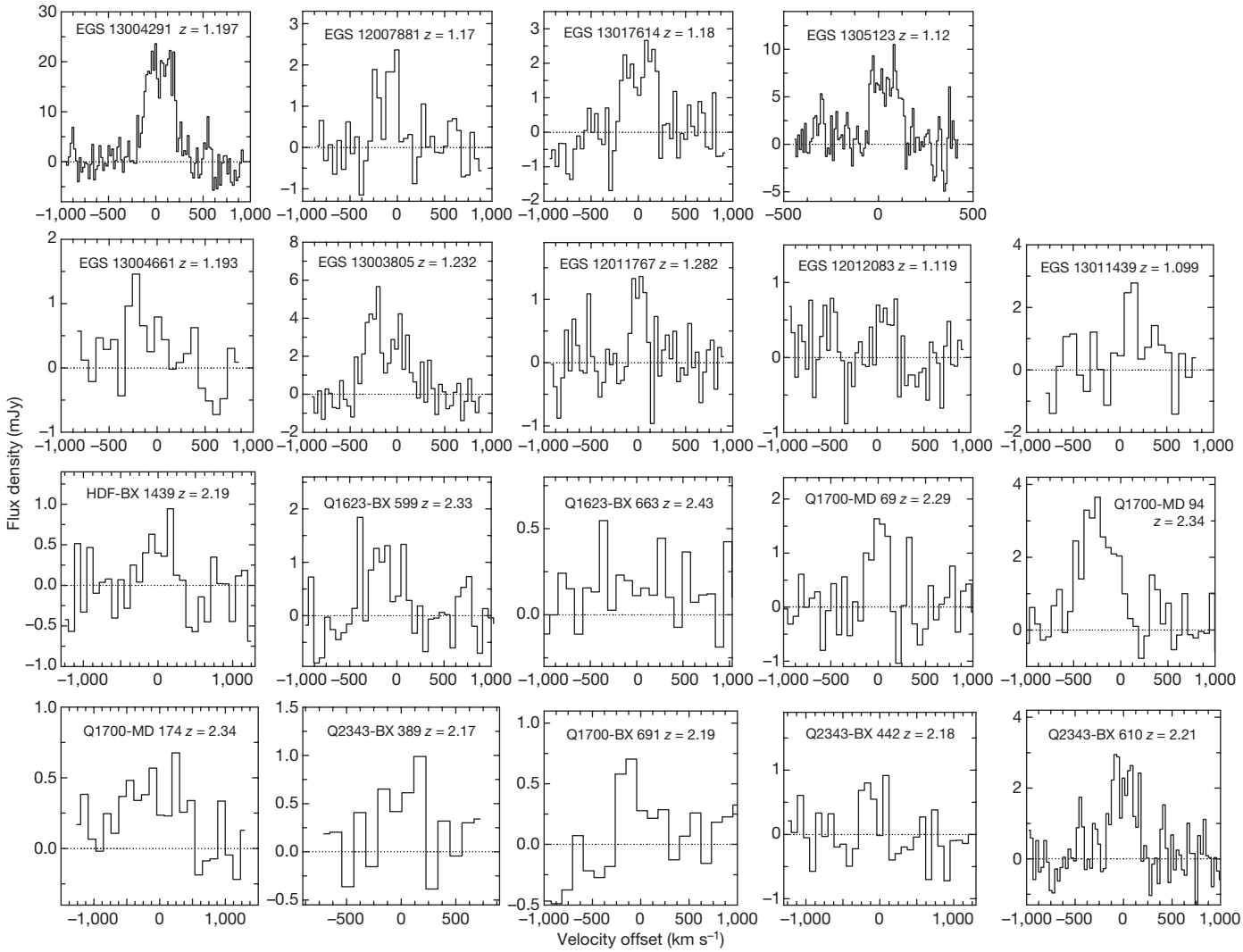

Figure 1 | Integrated CO spectra. The 0.87 mm CO $J = 3$–2 rotational line spectra in typical SFGs at z>1. The $z \approx 1.2$ SFGs were selected from the DEEP2/AEGIS survey[28] by taking SFGs with a stellar mass $M_* > 3 \times 10^{10}\,M_\odot$ and a star formation rate SFR $\geq 40\,M_\odot\,\mathrm{yr}^{-1}$ (Supplementary Information section 1), and without major galaxy–galaxy interactions. The $z \approx 2.3$ SFGs were selected from the Hα survey of BX UV-bright SFGs[20,29], with the same mass and star formation selection as at $z \approx 1.2$. The $<z> \approx 1.2$ (2.3) SFGs have mean stellar masses and star formation rates of $<\log[M_*\,(M_\odot)]> = 11.11$ (11.03) and $<\log[\mathrm{SFR}\,(M_\odot\,\mathrm{yr}^{-1})]> = 1.98$ (2.13) (Chabrier[27] initial stellar mass function) and sample the 'main sequence' of SFGs (Supplementary Fig. 1).

SFGs[10], we might expect between 1/3 and 2/3 of our massive $z \approx 2$ SFGs to be rotating disks, similar to, but probably more turbulent ($v_d/\sigma \approx 2$–6) than, the $z \approx 1$ AEGIS galaxies. Future sub-arcsecond CO measurements will be necessary to reveal the molecular gas kinematics in these systems.

Our spatially resolved observations of EGS 1305123 and the flux ratios of different CO lines in another $z \approx 1.5$ SFG[11,12] are consistent with the CO emission in these systems arising in giant molecular cloud systems of temperature ~10–25 K and mean gas densities of $<n(\mathrm{H_2})> \approx 10^2\,\mathrm{cm}^{-3}$, comparable to the Milky Way and $z \approx 0$ SFGs[13–15]. In normal $z \approx 0$ SFGs, the CO line luminosity L'_{CO} (in units of $\mathrm{K\,km\,s^{-1}\,pc^2}$) is proportional to the total cold (molecular hydrogen, plus helium) gas mass $M_{\mathrm{mol\text{-}gas}}$. A similar 'Galactic' conversion factor appears to be also justified for the $z \approx 1$–2 SFGs considered here, given (1) the similar extended structure with large molecular cloud complexes and (2) the comparable gas and star formation surface densities and near-solar metallicities of the $z \approx 1$–2 SFGs and the extragalactic star forming clouds studied in refs 13–15. In fact, a Galactic conversion factor may underestimate, rather than overestimate, the total cold molecular gas masses (Supplementary Information section 3)[15]. Figure 3a–c shows the gas fractions derived in this way from Table 1 for all 19 $z \approx 1$–2 SFGs (using 3σ upper limits for the non-detections), and four SFGs from the literature[11,16,17].

The molecular gas fractions, defined as the ratio of gas mass to the sum of gas and stellar mass, range broadly from 0.2 to 0.8, with an average of $<f_{\mathrm{mol\text{-}gas}}> \approx 0.44$ (Fig. 3). SFGs at $z = 1$–2 are three to ten times more gas-rich than $z \approx 0$ SFGs with $\log M_* \approx 10.5$–11 ($<f_{\mathrm{mol\text{-}gas}}$ (spirals)$> \approx 0.04$–0.1)[6,18,19]. Our survey thus provides direct and statistically significant (~7–10 σ in the uncertainty of the mean, for a constant CO-H_2 conversion factor) empirical evidence for the long-standing expectation that high-z SFGs are much more gas rich than $z \approx 0$ galaxies[9–12,20–23]. Within the uncertainties, the gas fractions do not depend much on galaxy selection method, star formation rate, or mass (Supplementary Information sections 1 and 3). There appears to be a marginally significant trend (2.8σ in the uncertainty of the mean) that the $z \approx 2$ SFGs are slightly more gas rich than those of similar mass at $z = 1$, with average values of $<f_{\mathrm{mol\text{-}gas}}> \approx 0.44$ and 0.34, respectively, broadly consistent with theoretical expectations (see below).

We note that our sample is still limited, and probes galaxies at the massive tail of the SFG populations in both redshift ranges (Supplementary Fig. 1). Although the relative trends appear robust, the uncertainty in the derived absolute value of the gas fraction in each galaxy is substantial, because of the combined uncertainties in

Table 1 | Properties of high-*z* SFGs

Source	z	v_d* (km s^{-1})	$R_{1/2}$† (kpc)	SFR‡ ($M_\odot$ yr^{-1})	$F_{CO\ 3\text{-}2}$§ (Jy km s^{-1})	$L_{CO\ 3\text{-}2}$‖ (K km s^{-1} pc^2)	$M_{mol\text{-}gas}$¶ ($M_\odot$)	M_*☆ ($M_\odot$)	f_{gas}#
EGS 13004291	1.20	300	7.2	172(86)	3.7(0.15)	$3.2(0.13)\times10^{10}$	$2.8(0.11)\times10^{11}$	$3.3(1.3)\times10^{11}$	0.46(0.19)
EGS 12007881	1.17	180	8.7	91(46)	1.15(0.06)	$9.4(0.49)\times10^{9}$	$8.3(0.43)\times10^{10}$	$1.6(0.64)\times10^{11}$	0.34(0.14)
EGS 13017614	1.18	270	6.6	74(37)	1.25(0.10)	$1.1(0.08)\times10^{10}$	$9.3(0.74)\times10^{10}$	$1.1(0.42)\times10^{11}$	0.47(0.19)
EGS 13035123	1.12	205	9.0	126(63)	1.9(0.05)	$1.4(0.04)\times10^{10}$	$1.3(0.03)\times10^{11}$	$3.4(1.4)\times10^{11}$	0.27(0.11)
EGS 13004661	1.19	180	6.6	82(41)	0.32(0.06)	$2.8(0.52)\times10^{9}$	$2.4(0.46)\times10^{10}$	$3.0(1.2)\times10^{10}$	0.45(0.20)
EGS 13003805	1.23	200	6.0	128(64)	2.25(0.15)	$2.0(0.14)\times10^{10}$	$1.8(0.12)\times10^{11}$	$2.1(0.84)\times10^{11}$	0.46(0.19)
EGS 12011767	1.28	80	7.0	47(24)	0.30(0.06)	$2.9(0.59)\times10^{9}$	$2.6(0.52)\times10^{10}$	$1.2(0.48)\times10^{11}$	0.18(0.08)
EGS 12012083	1.12	110	4.6	103(52)	<0.13(0.04)	$<9.9(3.3)\times10^{8}$	$<8.7(2.9)\times10^{9}$	$5.2(2.1)\times10^{10}$	<0.14(0.07)
EGS 13011439	1.10	94	4.6	90(45)	0.70(0.15)	$5.1(1.1)\times10^{9}$	$4.5(0.97)\times10^{10}$	$1.3(0.5)\times10^{11}$	0.26(0.12)
HDF-BX 1439	2.19	265	8.0	97(43)	0.23(0.08)	$6.6(2.2)\times10^{9}$	$5.9(1.9)\times10^{10}$	$5.7(2.3)\times10^{10}$	0.51(0.26)
Q1623-BX 599	2.33	265	2.8	127(50)	0.60(0.1)	$1.8(0.3)\times10^{10}$	$1.6(0.26)\times10^{11}$	$5.7(2.3)\times10^{10}$	0.73(0.32)
Q1623-BX 663	2.43	256	5.5	131(49)	<0.18(0.06)	$<5.7(1.9)\times10^{9}$	$<5.1(1.7)\times10^{10}$	$6.9(2.8)\times10^{10}$	<0.42(0.22)
Q1700-MD 69	2.29	217	9.4	141(75)	0.42(0.06)	$1.2(0.17)\times10^{10}$	$1.1(0.15)\times10^{11}$	$1.9(0.74)\times10^{11}$	0.36(0.15)
Q1700-MD 94	2.34	217	9.6	382(171)	2.0(0.3)	$6.0(0.9)\times10^{10}$	$5.3(0.79)\times10^{11}$	$1.5(0.61)\times10^{11}$	0.78(0.33)
Q1700-MD 174	2.34	240	3.6	117(57)	0.60(0.08)	$1.8(0.24)\times10^{10}$	$1.6(0.21)\times10^{11}$	$2.4(0.94)\times10^{11}$	0.4(0.17)
Q1700-BX 691	2.19	238	6.7	62(27)	0.15(0.05)	$4.0(1.2)\times10^{9}$	$3.5(1.1)\times10^{10}$	$7.6(3.0)\times10^{10}$	0.32(0.16)
Q2343-BX 389	2.17	259	4.2	235(86)	<0.15(0.05)	$<3.8(1.3)\times10^{9}$	$<3.3(1.1)\times10^{10}$	$6.9(2.8)\times10^{10}$	<0.33(0.17)
Q2343-BX 442	2.18	238	6.7	92(45)	0.43(0.08)	$1.1(0.21)\times10^{10}$	$1.0(0.19)\times10^{11}$	$1.5(0.59)\times10^{11}$	0.41(0.18)
Q2343-BX 610	2.21	324	4.6	141(63)	0.95(0.08)	$2.6(0.22)\times10^{10}$	$2.3(0.19)\times10^{11}$	$1.7(0.68)\times10^{11}$	0.57(0.23)

For details see Supplementary Information sections 1–3.
* Maximum intrinsic rotation velocity.
† Half-light radius.
‡ Extinction corrected star formation rates (and 1σ r.m.s. uncertainties) from a combination of UV/optical continuum, Hα and 24 μm continuum, adopting a Chabrier[27] initial stellar mass function.
§ Source and line integrated CO 3–2 flux with 1σ r.m.s. uncertainties in parentheses. Upper limits are 3σ rms.
‖ $L_{CO\ 3\text{-}2} = 3.25\times10^{13}\,F_{CO\ 3\text{-}2}\,(D_L)^2(1+z)^{-3}(\nu_{3\text{-}2,obs})^{-2}$, where $L_{CO\ 3\text{-}2}$ is in units of K km s^{-1} pc^2, D_L is the luminosity distance of the source (in Gpc), and $\nu_{3\text{-}2,obs}$ is the observed line frequency of the 3–2 line (in GHz).
¶ Total H_2 + He mass in cold gas (=1.36 times the H_2 mass), assuming $X = N(H_2)/I(CO) = 2\times10^{20}$ cm^{-2} K^{-1} km^{-1} s, or $\alpha = M(H_2)/L_{CO\ 1\text{-}0} = 3.2$, where X and α are the CO-H_2 conversion factor in terms of gas surface density (X) and mass (α), determined from CO 3–2 luminosity and a correction $I(CO\ 1\text{–}0)/I(CO\ 3\text{–}2) = 2$. The 1$\sigma$ r.m.s. uncertainties are in parentheses, and upper limits are 3σ r.m.s.
☆ Stellar mass (and 1σ r.m.s. uncertainties) determined from population synthesis modelling to the rest-frame UV to infrared spectral energy distribution, assuming a Chabrier[27] initial stellar mass function.
$f_{mol\text{-}gas} = M_{mol\text{-}gas}/(M_{mol\text{-}gas} + M_*)$, upper limits are 3$\sigma$ r.m.s.

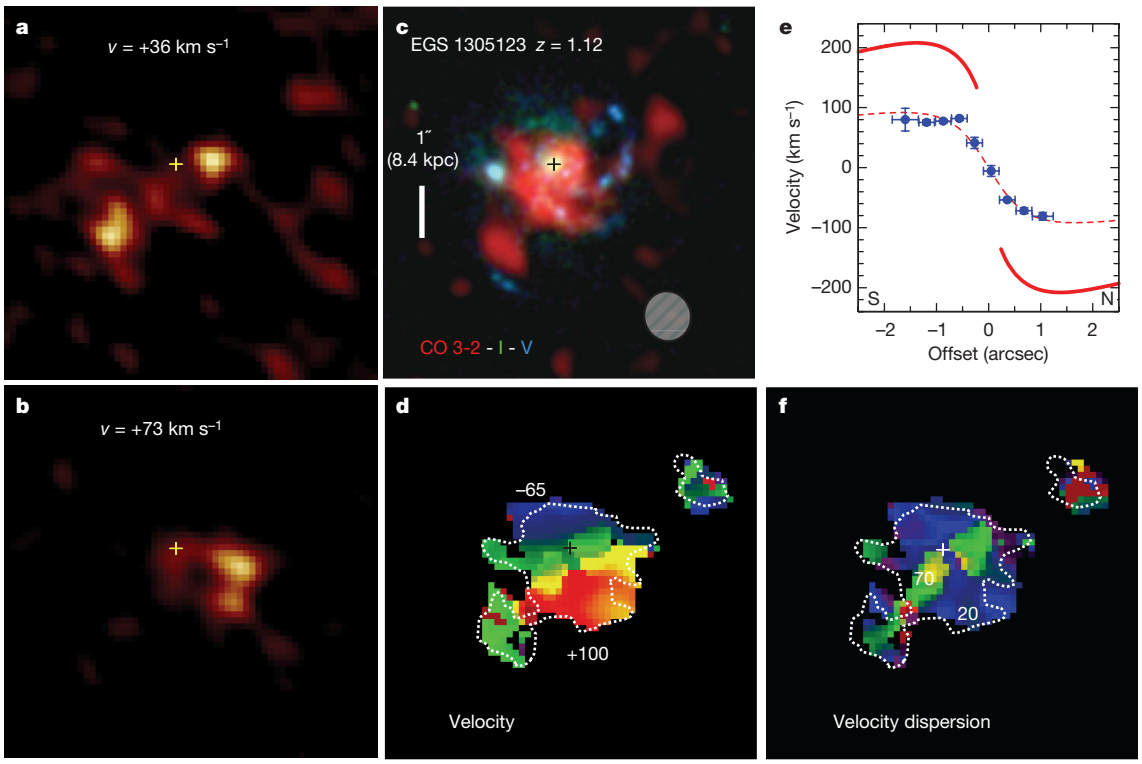

Figure 2 | CO maps in EGS 1305123. High resolution (FWHM 0.6″ × 0.7″) CO 3–2 maps and rotation curve in the $z = 1.12$ AEGIS galaxy EGS 1305123, obtained at ~2 mm with the IRAM PdBI in A-configuration[30]. **a**, **b**, Examples of two CO 3–2 maps in 9 km s^{-1} channels at +36 km s^{-1} (**a**) and +72 km s^{-1} (**b**); the r.m.s. uncertainty in these channel maps is 0.3 mJy. The channel maps show several massive molecular clumps. The three bright clumps in **a** have fluxes of 1.7, 1.7 and 1.1 mJy, or 5.7, 5.7 and 3.7 σ r.m.s., respectively. The three brightest clumps visible in **b** have fluxes of 2.4, 2.1 and 1.45 mJy, or 8, 7 and 4.8 σ r.m.s., respectively. Typical gas masses in the clumps are ~$5\times10^9\,M_\odot$, with intrinsic radii of <1–2 kpc, gas surface densities >300–700 $M_\odot$ pc^{-2} and velocity dispersions ~19 km s^{-1}. **c**, CO integrated line emission (red), I-band (green) and V-band (blue) HST ACS images of the source. Hatched ellipse, CO beam size; cross, position of nucleus. **d**, **f**, Peak velocity (**d**) and velocity dispersion (**f**) maps of the CO emission, obtained from Gaussian fits to the line emission in each spatial point of the map. Dotted white line, outline of the integrated emission; cross, position of nucleus. **e**, Peak CO velocity (and 1σ r.m.s. fitting uncertainty error bars) along the major axis (position angle 16° east of north) of the galaxy. Dashed red curve, best fitting exponential disk model with radial scale length R_d=0.77″ and dynamical mass of $2\times10^{11}\,M_\odot$, for an adopted inclination of 27°. Continuous red curve, intrinsic rotation curve of this model as a function of radius.

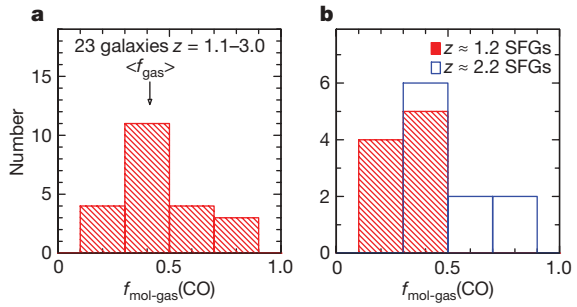

Figure 3 | High molecular gas fractions in SFGs at high *z*. **a**, The distribution of molecular gas fractions for all 23 SFGs with good stellar mass estimates from $z \approx 1$ to $z \approx 3.0$. **b**, A comparison of the distribution of molecular gas fractions for the $z \approx 1.2$ (red) and $z \approx 2.2$ (blue) SFGs from this study. We define $f_{mol\text{-}gas} = M_{gas}/(M_* + M_{gas})$. The molecular gas mass and fractions include a correction of 1.36 for helium.

the CO-H_2 conversion factor (Supplementary Information section 3) and stellar masses, each at least ±50%. Larger samples will be needed to confirm the tantalizing redshift trend in Fig. 3b.

The high gas fractions at $z \approx 2$ and $z \approx 1$ (separated by a cosmic time of ~2.5 Gyr) are impressive, especially considering that the halo masses of most galaxies probably exceed $10^{12}\,M_{\odot}$. These masses are close to or above the 'quenching mass', $M_t \approx 5 \times 10^{11}\,M_{\odot}$, at which the gas becomes hot and accretion inefficient[22–25]. The gas exhaustion timescales of our sample galaxies, $t_{exhaust} = M_{mol\text{-}gas}/SFR$ (where SFR is the star formation rate), are ~0.9 Gyr (dispersion ±0.6 Gyr) for the $z \approx 1$–2 SFGs, assuming that the SFR continues at the current rate. These timescales are significantly shorter than the cosmic interval between $z \approx 2$ and $z \approx 1$, suggesting that either some replenishment is required during this epoch, or that the two samples have experienced different accretion and evolution histories. Our finding is consistent with simulations predicting that rapid accretion of cold gas can exist above M_t and supplies the growing galaxies at high-z semi-continuously with fresh baryonic gas[21–23]. Our observations require that efficient feeding must continue in at least some massive galaxies to $z \approx 1$ (Supplementary Information section 4). Given their stellar masses and star formation rates, it is possible that some of the $z \approx 1.2$ galaxies are descendents of the types of galaxies we sample at $z \approx 2.3$. Current work on hydro-dynamical and semi-analytical simulations, including baryonic gas physics, star formation and feedback, predict average gas fractions similar to or somewhat lower than the observations in Fig. 3 (25–45% at $z \approx 2$, 10–40% at $z \approx 1$–1.5: R. Davé *et al.*, manuscript in preparation; Q. Guo and S. D. M. White, manuscript in preparation; P. Ocvirk *et al.*, manuscript in preparation), all of which predict semi-continuous re-supply of the evolving galaxies with fresh gas from their surrounding cosmic web. This agreement between theory and observations is encouraging in terms of an overall emerging picture of galaxy formation.

A quantitative analysis of the data in Table 1 demonstrates that the large star formation rates at $z \approx 1$–2 (refs 1, 2) are the consequence of the large molecular gas reservoirs and not of a greater star formation efficiency than at $z \approx 0$. To within the uncertainties, the so called 'Kennicutt-Schmidt' relation[26] between star formation rate and gas surface densities appears to be independent of redshift (L.J.T. *et al.*, manuscript in preparation).

Received 3 September; accepted 22 December 2009.

1. Noeske, K. G. *et al.* Star formation in AEGIS field galaxies since z=1.1: the dominance of gradually declining star formation, and the main sequence of star-forming galaxies. *Astrophys. J.* **660,** L43–L46 (2007).
2. Daddi, E. *et al.* Multiwavelength study of massive galaxies at z~2. I. Star formation and galaxy growth. *Astrophys. J.* **670,** 156–172 (2007).
3. Greve, T. R. *et al.* An interferometric CO survey of luminous submillimetre galaxies. *Mon. Not. R. Astron. Soc.* **359,** 1165–1183 (2005).
4. Combes, F. *et al.* High resolution observations of a starburst at z = 0.223: resolved CO(1-0) structure. *Astron. Astrophys.* **460,** L49–L52 (2006).
5. Tacconi, L. J. *et al.* Submillimeter galaxies at z ~ 2: evidence for major mergers and constraints on lifetimes, IMF, and CO-H_2 conversion factor. *Astrophys. J.* **680,** 246–262 (2008).
6. Leroy, A., Bolatto, A. D., Simon, J. D. & Blitz, L. The molecular interstellar medium of dwarf galaxies on kiloparsec scales: a new survey for CO in northern, IRAS-detected dwarf galaxies. *Astrophys. J.* **625,** 763–784 (2005).
7. Rand, R. J. & Kulkarni, S. R. M51: molecular spiral arms, giant molecular associations and superclouds. *Astrophys. J.* **349,** L43–L46 (1990).
8. Rand, R. J., Kulkarni, S. R. & Rice, W. Star formation and the distribution of HI and infrared emission in M51. *Astrophys. J.* **390,** 66–78 (1992).
9. Förster Schreiber, N. M. *et al.* SINFONI integral field spectroscopy of z~2 UV-selected galaxies: rotation curves and dynamical evolution. *Astrophys. J.* **645,** 1062–1075 (2006).
10. Förster Schreiber, N. M. *et al.* The SINS survey: SINFONI integral field spectroscopy of z ~ 2 star-forming galaxies. *Astrophys. J.* **706,** 1364–1428 (2009).
11. Daddi, E. *et al.* Vigorous star formation with low efficiency in massive disk galaxies at z = 1.5. *Astrophys. J.* **673,** L21–L24 (2008).
12. Dannerbauer, H. *et al.* Low, Milky-Way-like molecular gas excitation of massive disk galaxies at z~1.5. *Astrophys. J.* **698,** L178–L182 (2009).
13. Solomon, P. M., Rivolo, A. R., Barrett, J. & Yahil, A. Mass, luminosity, and line width relations of Galactic molecular clouds. *Astrophys. J.* **319,** 730–741 (1987).
14. Dickman, R. L., Snell, R. L. & Schloerb, F. P. Carbon monoxide as an extragalactic mass tracer. *Astrophys. J.* **309,** 326–330 (1986).
15. Bolatto, A. D., Leroy, A. K., Rosolowsky, E., Walter, F. & Blitz, L. The resolved properties of extragalactic giant molecular clouds. *Astrophys. J.* **686,** 948–965 (2008).
16. Baker, A. J., Tacconi, L. J., Genzel, R., Lehnert, M. D. & Lutz, D. Molecular gas in the lensed Lyman break galaxy cB58. *Astrophys. J.* **604,** 125–140 (2004).
17. Coppin, K. E. K. *et al.* A detailed study of gas and star formation in a highly magnified Lyman break galaxy at z = 3.07. *Astrophys. J.* **665,** 936–943 (2007).
18. Sage, L. J. Molecular gas in nearby galaxies I. CO observations of a distance-limited sample. *Astron. Astrophys.* **272,** 123–136 (1993).
19. Young, J. S. & Scoville, N. Z. Molecular gas in galaxies. *Annu. Rev. Astron. Astrophys.* **29,** 581–625 (1991).
20. Erb, D. K. *et al.* Hα observations of a large sample of galaxies at z ~ 2: implications for star formation in high-redshift galaxies. *Astrophys. J.* **647,** 128–139 (2006).
21. Kereš, D., Katz, N., Weinberg, D. H. & Davé, R. How do galaxies get their gas? *Mon. Not. R. Astron. Soc.* **363,** 2–28 (2005).
22. Ocvirk, P., Pichon, C. & Teyssier, R. Bimodal gas accretion in the Horizon-Mare Nostrum galaxy formation simulation. *Mon. Not. R. Astron. Soc.* **390,** 1326–1338 (2008).
23. Dekel, A. *et al.* Cold streams in early massive hot haloes as the main mode of galaxy formation. *Nature* **457,** 451–454 (2009).
24. White, S. D. M. & Rees, M. J. Core condensation in heavy halos — A two-stage theory for galaxy formation and clustering. *Mon. Not. R. Astron. Soc.* **183,** 341–358 (1978).
25. Birnboim, Y. & Dekel, A. Virial shocks in galactic haloes? *Mon. Not. R. Astron. Soc.* **345,** 349–364 (2003).
26. Kennicutt, R. C. The global Schmidt Law in star-forming galaxies. *Astrophys. J.* **498,** 541–552 (1998).
27. Chabrier, G. Galactic stellar and substellar initial mass function. *Publ. Astron. Soc. Pacif.* **115,** 763–795 (2003).
28. Davis, M. *et al.* The All-Wavelength Extended Groth Strip International Survey (AEGIS) data sets. *Astrophys. J.* **660,** L1–L6 (2007).
29. Steidel, C. C. *et al.* A survey of star-forming galaxies in the 1.4<~z<~ 2.5 redshift desert: overview. *Astrophys. J.* **604,** 534–550 (2004).
30. Cox, P. (ed.) *IRAM Annual Report 2006* (IRAM, Grenoble, 2006); *IRAM Annual Report 2007* (IRAM, Grenoble, 2007); available at ⟨http://iram.fr/IRAMFR/ARN/AnnualReports/Years.html⟩.

Supplementary Information is linked to the online version of the paper at www.nature.com/nature.

Acknowledgements This work is based on observations carried out with the IRAM Plateau de Bure Interferometer. IRAM is supported by INSU/CNRS (France), MPG (Germany) and IGN (Spain). We thank B. Lazareff and the IRAM staff for their work in developing the new PdBI receiver systems, which made these technically difficult observations feasible. We are grateful to J. Blaizot, L.-M. Dansac, R. Davé, D. Kereš, P. Ocvirk, C. Pichon and R. Teyssier for communicating unpublished results of their simulations and for discussions. A.B. and T.N. thank the Cluster of Excellence "Origin and Structure of the Universe" for support. M.C.C. is a Spitzer Fellow; A.B. is a Max Planck Fellow.

Author Contributions All authors have contributed extensively to this manuscript.

Author Information Reprints and permissions information is available at www.nature.com/reprints. The authors declare no competing financial interests. Correspondence and requests for materials should be addressed to L.J.T. (linda@mpe.mpg.de).